
Article:
Liang, Y., Cui, W., Shen, Q. et al. (2 more authors) (2021) Cramr-Rao bound for DOA estimation exploiting multiple frequency pairs. IEEE Signal Processing Letters, 28. pp. 1210-1214. ISSN 1070-9908

https://doi.org/10.1109/lsp.2021.3088051

Cramér-Rao Bound for DOA Estimation Exploiting Multiple Frequency Pairs

Yibao Liang, Wei Cui, Qing Shen, Wei Liu, *Senior Member, IEEE,* Hantian Wu

***Abstract*—The Cramér-Rao bound (CRB) for direction of arrival (DOA) estimation exploiting both auto-correlation and cross-correlation information within multiple frequencies of the received array signals is derived. It provides a tighter bound than the existing CRB for the dual-frequency scenario. For the multiple frequencies, it is much lower than its dual-frequency counterpart, and also exists for a greater number of sources, thereby validating that exploiting multiple frequency pairs can improve both estimation accuracy and target resolvability.**

***Index Terms*—Direction-of-arrival (DOA) estimation, Cramér-Rao bound (CRB), multiple frequencies, underdetermined.**

I. Introduction

In recent years, direction of arrival (DOA) estimation in the underdetermined case, where the number of sources is larger than that of physical sensors, has attracted a lot of research interest. A variety of sparse array structures [1]–[9] have been proposed to provide enhanced degrees of freedom (DOFs), based on which high-resolution techniques [1], [10], [11] can be implemented to solve the problem. The performance of existing algorithms has been well-studied [12]–[16] through analyzing the celebrated Cramér-Rao bound (CRB), a lower bound on the variance of any unbiased estimator.

For signals embracing frequency diversity, multiple frequency components can be utilized to improve target resolvability and estimation accuracy, while simultaneously reducing system complexity. Based on auto-correlation information where the cross-correlation information across frequencies is ignored, a number of underdetermined methods using sparse arrays have been proposed [17]–[22], with the corresponding CRB derived in our earlier work [23], [24]. Furthermore, based on the ensured correlation property among different frequencies, even more sources can be resolved by a uniform linear array (ULA) [25]–[30]. The key idea lies in extending the concept of physical sparse arrays to the joint spatio-spectral domain.

To assess the performance of the derived algorithms employing two coprime frequencies [25], a CRB result was presented in [31]; however, it relies on the *a priori* knowledge that signals at the second frequency are phase-delayed versions of those at the first frequency, at every time instant. In practice, this is not always true, and it is not utilized by algorithms developed for this scenario, e.g., [25]–[28]; instead, group sparsity is commonly employed to jointly estimate the DOAs. Moreover, the frequency-dependent radar cross section (RCS) fluctuations may also impair the validity of this assumption. These factors imply that the CRB in [31] may not be tight enough for the dual-frequency scenario. To the best of our knowledge, the performance bound for underdetermined DOA estimation exploiting multiple frequency pairs is still unknown.

The objective of this letter is to derive a general CRB result for DOA estimation exploiting both auto-correlation and cross-correlation information within multiple frequencies. First, a practical multi-frequency signal model is introduced involving time-variant phase differences among frequencies and amplitude variations induced by RCS fluctuations. Then, a closed-form CRB expression is derived for the DOA-related block through the partitioned inverse of the Fisher information matrix (FIM), where information across multiple frequencies is exploited. This result fits both the spatio-temporal and spatio-frequency domain data, regardless of the array geometry. Compared to that in [31] for the dual-frequency scenario, our CRB is tighter for assessing the performance of existing methods [25]–[28]. Theoretical analyses and simulation results are provided to illustrate the superior estimation accuracy and target resolvability by utilizing multiple frequency pairs.

II. Preliminaries

A. Signal Model

Consider an array of M omnidirectional sensors with identical responses. It receives L signals reflected by K far-field targets located at K distinct directions $\boldsymbol{\theta} = [\theta_1, \ldots, \theta_K]^T$, with $(\cdot)^T$ denoting the transpose operator. Let f_l with $l = 1, \ldots, L$ denote the transmitted carrier frequencies, and then the echo signals associated with frequency f_l can be modeled as

$$\breve{\boldsymbol{x}}_l(t) = \mathrm{e}^{\mathrm{j}2\pi f_l t} \sum_{k=1}^{K} s_k^{(l)}(t)\boldsymbol{a}_l(\theta_k) + \breve{\boldsymbol{n}}_l(t), \tag{1}$$

where $s_k^{(l)}(t)$ is the k-th baseband source signal at frequency f_l, $\breve{\boldsymbol{n}}_l(t)$ is the additive noise, and $\boldsymbol{a}_l(\theta_k)$ the steering vector.

The echo signals are first converted to baseband and then low-pass filtered, yielding

$$\boldsymbol{x}_l(t) = \sum_{k=1}^{K} s_k^{(l)}(t)\boldsymbol{a}_l(\theta_k) + \boldsymbol{n}_l(t) = \boldsymbol{A}_l\boldsymbol{s}_l(t) + \boldsymbol{n}_l(t), \tag{2}$$

where $\boldsymbol{A}_l = [\boldsymbol{a}_l(\theta_1), \ldots, \boldsymbol{a}_l(\theta_K)]$ is an $M \times K$ array manifold matrix corresponding to f_l (the dependence on $\boldsymbol{\theta}$ is dropped for simplicity), and $\boldsymbol{s}_l(t) = [s_1^{(l)}(t), \ldots, s_K^{(l)}(t)]^T$.

This work was supported in part by the National Natural Science Foundation of China under Grants 61801028 and 61628101. (Corresponding author: Qing Shen.)

Y. Liang, W. Cui, Q. Shen, and H. Wu are with the School of Information and Electronics, Beijing Institute of Technology, Beijing, 100081, China (e-mail: liangyibao@bit.edu.cn, cuiwei@bit.edu.cn, qing-shen@outlook.com, wuhantian97@163.com).

W. Liu is with the Department of Electronic and Electrical Engineering, University of Sheffield, Sheffield, S1 3JD, UK (e-mail: w.liu@sheffield.ac.uk).

Stacking the data at L frequencies, we have $\bar{\boldsymbol{x}}(t) = [\boldsymbol{x}_1^T(t), \ldots, \boldsymbol{x}_L^T(t)]^T$, $\bar{\boldsymbol{A}} = \text{blkdiag}(\boldsymbol{A}_1, \ldots, \boldsymbol{A}_L)$, $\bar{\boldsymbol{s}}(t) = [\boldsymbol{s}_1^T(t), \ldots, \boldsymbol{s}_L^T(t)]^T$, and $\bar{\boldsymbol{n}}(t) = [\boldsymbol{n}_1^T(t), \ldots, \boldsymbol{n}_L^T(t)]^T$, with blkdiag$(\cdot)$ being the block diagonalizing operator. Thus,

$$\bar{\boldsymbol{x}}(t) = \bar{\boldsymbol{A}}\bar{\boldsymbol{s}}(t) + \bar{\boldsymbol{n}}(t). \tag{3}$$

In practice, frequency-dependent RCS fluctuations will induce amplitude variations in the echo signals, leading to

$$s_k^{(l)}(t) = \rho_k^{(l)}(t) y_k^{(l)}(t), \tag{4}$$

where $\rho_k^{(l)}(t)$ is a real-valued positive amplitude variation coefficient, and $y_k^{(l)}(t)$ denotes the uncontaminated transmitted signal at f_l. Moreover, due to differences in propagation delay and target reflectivity, an additional unknown phase difference (probability time-variant) arises between the uncontaminated signals at different frequencies [28]. Choosing f_1 as the reference, we can write

$$y_k^{(l)}(t) = \mathrm{e}^{\mathrm{j}\phi_k^{(l)}(t)} y_k^{(1)}(t), \tag{5}$$

where $\phi_k^{(l)}(t)$ denotes the phase difference w.r.t. f_1, with $\phi_k^{(1)}(t) = 0$.

B. Second-Order Statistical Characteristics

The following assumptions are introduced regarding the statistical properties of the data:

- **A1** The signals are random processes with zero mean, i.e., $E[y_k^{(l)}(t)] = 0$ and $E[s_k^{(l)}(t)] = 0$. For a fixed l, $\{s_k^{(l)}(t)\}_{k=1}^K$ are uncorrelated due to target motion or RCS fluctuations (Swerling II [28], [32]).
- **A2** $\{\boldsymbol{n}_l(t)\}_{l=1}^L$ are spatially and temporally white, Gaussian distributed with zero mean, mutually uncorrelated, independent from the signals.
- **A3** $\{f_l\}_{l=1}^L$ lie in the same RCS frequency region in general [33], so that the fluctuating RCS values for a fixed k share the same mean value and variance.
- **A4** $\{\rho_k^{(l)}(t)\}_{l=1}^L$ and $\{\phi_k^{(l)}(t)\}_{l=1}^L$ are stationary, mutually independent, random processes with finite means and variances, also uncorrelated with the signals.

Define the covariance matrices of $\bar{\boldsymbol{x}}(t)$, $\bar{\boldsymbol{s}}(t)$, and $\bar{\boldsymbol{n}}(t)$ as $\bar{\boldsymbol{R}} \triangleq E[\bar{\boldsymbol{x}}(t)\bar{\boldsymbol{x}}^H(t)]$, $\bar{\boldsymbol{P}} \triangleq E[\bar{\boldsymbol{s}}(t)\bar{\boldsymbol{s}}^H(t)]$, and $\bar{\boldsymbol{Q}} \triangleq E[\bar{\boldsymbol{n}}(t)\bar{\boldsymbol{n}}^H(t)]$, respectively, with $E[\cdot]$ denoting the expectation operator and $(\cdot)^H$ being the Hermitian transpose operator.

According to **A1** and **A2**, it follows from (3) that

$$\bar{\boldsymbol{R}} = \bar{\boldsymbol{A}}\bar{\boldsymbol{P}}\bar{\boldsymbol{A}}^H + \bar{\boldsymbol{Q}}, \tag{6}$$

where the (i,l)-th $(i,l = 1, \ldots, L)$ block of $\bar{\boldsymbol{R}}$ is defined as

$$\boldsymbol{R}_{i,l} \triangleq E[\boldsymbol{x}_i(t)\boldsymbol{x}_l^H(t)] = \boldsymbol{A}_i \boldsymbol{P}_{i,l} \boldsymbol{A}_l^H + \boldsymbol{Q}_{i,l}. \tag{7}$$

Herein, $\boldsymbol{P}_{i,l}$ and $\boldsymbol{Q}_{i,l}$ are respectively defined as

$$\begin{aligned} \boldsymbol{P}_{i,l} &\triangleq E[\boldsymbol{s}_i(t)\boldsymbol{s}_l^H(t)] = \text{diag}(\boldsymbol{p}_{i,l}), \\ \boldsymbol{Q}_{i,l} &\triangleq E[\boldsymbol{n}_i(t)\boldsymbol{n}_l^H(t)] = \begin{cases} \sigma_l \boldsymbol{I}_M, & \text{for } i = l, \\ \boldsymbol{0}, & \text{for } i \neq l, \end{cases} \end{aligned} \tag{8}$$

where diag$(\cdot)$ is a diagonal matrix whose diagonal entries are given by the input vector, σ_l is the noise power at f_l, $\boldsymbol{p}_{i,l} = [p_1^{(i,l)}, \ldots, p_K^{(i,l)}]^T$, and $\boldsymbol{I}_M$ is an $M \times M$ identity matrix.

The probability distributions of amplitude variations are determined by those of the RCS fluctuations [34, p. 2.21]. According to **A3**, for a fixed k, we have

$$E[\rho_k^{(i)}(t)] = E[\rho_k^{(l)}(t)], \quad \text{var}[\rho_k^{(i)}(t)] = \text{var}[\rho_k^{(l)}(t)], \tag{9}$$

where var$[\cdot]$ denotes the variance of the input argument.

Using (9), for $1 \leq i \neq l \leq L$, we have

$$\begin{aligned} E[(\rho_k^{(i)})^2(t)] &= (E[\rho_k^{(i)}(t)])^2 + \text{var}[\rho_k^{(i)}(t)] \\ &= (E[\rho_k^{(l)}(t)])^2 + \text{var}[\rho_k^{(l)}(t)] = E[(\rho_k^{(l)})^2(t)]. \end{aligned} \tag{10}$$

Using **A4**, (4), and (5), we can write $E[s_k^{(l)}(t)]$ as

$$E[s_k^{(l)}(t)] = E[\rho_k^{(l)}(t)] E[\mathrm{e}^{\mathrm{j}\phi_k^{(l)}(t)}] E[y_k^{(1)}(t)]. \tag{11}$$

By (10) and (11), the following results are obtained:

$$\begin{aligned} p_k^{(i,i)} &= E[(\rho_k^{(i)})^2(t)] E[y_k^{(1)}(t)(y_k^{(1)})^*(t)] = p_k^{(l,l)}, \\ p_k^{(i,l)} &= E[\mathrm{e}^{\mathrm{j}\left(\phi_k^{(i)}(t) - \phi_k^{(l)}(t)\right)}] E[\rho_k^{(i)}(t)\rho_k^{(l)}(t)] \\ &\quad \cdot E[y_k^{(1)}(t)(y_k^{(1)})^*(t)] = (p_k^{(l,i)})^*, \text{ for } 1 \leq i \neq l \leq L. \end{aligned} \tag{12}$$

Extending (12) to all the K sources, we obtain

$$\boldsymbol{p}_{i,i} = \boldsymbol{p}_{l,l}, \quad \boldsymbol{p}_{i,l} = \boldsymbol{p}_{l,i}^*, \quad \text{for } 1 \leq i \neq l \leq L. \tag{13}$$

Note that entries in $\boldsymbol{p}_{i,l}$ $(i \neq l)$ are complex values, and are useful for underdetermined DOA estimation in the spatio-spectral domain [25]–[28]. Equation (13) is the basis for subsequent derivations, and the derived CRB results are valid as long as (13) holds. In particular, they can be easily extended to cases where the source powers across frequencies are proportional up to known coefficients (see [21]).

In active sensing, the transmitted signals for all targets are often identical, i.e., $y_k^{(l)}(t)$ is independent of k. The subscript k is introduced to cover cases where the signals are emitted by the targets directly. In such cases, the amplitude variation caused by RCS fluctuations vanishes, and thus **A3** should be replaced by a new assumption that the signals emitted by the same source share identical powers across frequencies.

III. Cramér-Rao Bound for DOA Estimation Exploiting Multiple Frequency Pairs

A. Derivation of the CRB

The CRB depends on the probability distribution of the data. Here $\bar{\boldsymbol{x}}(t)$ is assumed to be jointly Gaussian distributed, since the Gaussian distribution is commonly advocated in literature due to its mathematical convenience [35, p. 363] and practical value [36, p. 11]; moreover, for frequency-domain data, e.g., discrete Fourier transform results, it asymptotically follows the Gaussian distribution when the observation time is long enough [37, p. 94]. Hence, the Gaussian CRB fits not only spatio-temporal domain data, but also spatio-frequency domain data. In addition, it offers a starting point for further extension to complex elliptical symmetric distributions [38], [39].

The CRB can be obtained from the inverse of FIM. Let $\boldsymbol{\alpha}$ collect all the real-valued unknown parameters. Under the Gaussian distribution, a standard FIM formula for N i.i.d. snapshots is given by [40]:

$$\boldsymbol{F} = N \left(\boldsymbol{W} \frac{\partial \bar{\boldsymbol{r}}}{\partial \boldsymbol{\alpha}^T}\right)^H \left(\boldsymbol{W} \frac{\partial \bar{\boldsymbol{r}}}{\partial \boldsymbol{\alpha}^T}\right), \tag{14}$$

where $\boldsymbol{W} = \left(\bar{\boldsymbol{R}}^T \otimes \bar{\boldsymbol{R}}\right)^{-1/2}$ and $\bar{\boldsymbol{r}} = \mathrm{vec}(\bar{\boldsymbol{R}})$. Here, $\otimes$ denotes the Kronecker product, $\partial f(\boldsymbol{\alpha})/\partial \boldsymbol{\alpha}$ denotes the partial derivative of $f(\boldsymbol{\alpha})$ w.r.t. $\boldsymbol{\alpha}$, and $\mathrm{vec}(\cdot)$ is the vectorization operator. The $[L(L-1)K + 2K + L] \times 1$ unknown parameter vector is given by

$$\boldsymbol{\alpha} = \left[\boldsymbol{\theta}^T, \boldsymbol{\beta}^T\right]^T = \left[\boldsymbol{\theta}^T, \boldsymbol{p}_{1,1}^T, \mathrm{Re}(\bar{\boldsymbol{p}}^T), \mathrm{Im}(\bar{\boldsymbol{p}}^T), \boldsymbol{\sigma}^T\right]^T, \quad (15)$$

where $\bar{\boldsymbol{p}} = [\boldsymbol{p}_{1,2}^T, \ldots, \boldsymbol{p}_{1,L}^T, \boldsymbol{p}_{2,3}^T, \ldots, \boldsymbol{p}_{L-1,L}^T]^T$ and $\boldsymbol{\sigma} = [\sigma_1, \ldots, \sigma_L]^T$ with $\mathrm{Re}(\cdot)$ and $\mathrm{Im}(\cdot)$ denoting the real and imaginary parts of the input argument, respectively.

In general, only the CRB for DOAs is of interest. A closed-form CRB expression for the DOA-related block allows comparison with the asymptotic covariance matrix of estimation errors, and provides physical insights into the underlying problem. To this end, we introduce the following matrices:

$$\boldsymbol{G} = \boldsymbol{W}\frac{\partial \bar{\boldsymbol{r}}}{\partial \boldsymbol{\theta}^T}, \quad \boldsymbol{\Delta} = \boldsymbol{W}\frac{\partial \bar{\boldsymbol{r}}}{\partial \boldsymbol{\beta}^T}. \quad (16)$$

The dimensions of $\boldsymbol{G}$ and $\boldsymbol{\Delta}$ are $L^2M^2 \times K$ and $L^2M^2 \times [L(L-1)K + K + L]$, respectively. As such, (14) can be rewritten as $\boldsymbol{F} = N[\boldsymbol{G}, \boldsymbol{\Delta}]^H[\boldsymbol{G}, \boldsymbol{\Delta}]$. Assume that $\boldsymbol{F}$ is positive definite, and then the DOA-related block of the CRB can be obtained from the Schur complement of $\boldsymbol{\Delta}^H\boldsymbol{\Delta}$ [35]:

$$\boldsymbol{B} = \frac{1}{N}\left(\boldsymbol{G}^H\boldsymbol{\Pi}_{\boldsymbol{\Delta}}^{\perp}\boldsymbol{G}\right)^{-1}, \quad (17)$$

where $\boldsymbol{\Pi}_{\boldsymbol{\Delta}}^{\perp} = \boldsymbol{I}_{L^2M^2} - \boldsymbol{\Delta}(\boldsymbol{\Delta}^H\boldsymbol{\Delta})^{-1}\boldsymbol{\Delta}^H$ stands for the orthogonal projector onto the null space of $\boldsymbol{\Delta}^H$.

Introducing the column-blockwise vectorization operator, $\mathrm{vecb}(\cdot)$ [41, Eq. (2)], we can write $\bar{\boldsymbol{r}}$ as

$$\bar{\boldsymbol{r}} = \boldsymbol{J}\mathrm{vecb}(\bar{\boldsymbol{R}}) = \boldsymbol{J}\sum_{i=1}^{L}\sum_{l=1}^{L}(\boldsymbol{u}_{i,l} \otimes \boldsymbol{r}_{i,l}), \quad (18)$$

where $\boldsymbol{J} = \boldsymbol{I}_L \otimes \boldsymbol{\Omega}^{-1} \otimes \boldsymbol{I}_M$ and $\boldsymbol{u}_{i,l} = \mathrm{vec}(\boldsymbol{U}_{i,l})$. Herein, $\boldsymbol{J}$ is a permutation matrix. $\boldsymbol{\Omega}$ is an $LM \times LM$ commutation matrix defined in [42, p. 115]. $\boldsymbol{U}_{i,l}$ is an $L \times L$ matrix having a unit element at the (i,l)-th position and zeros elsewhere. In addition, $\boldsymbol{r}_{i,l}$ is expressed as

$$\boldsymbol{r}_{i,l} = \mathrm{vec}(\boldsymbol{R}_{i,l}) = \begin{cases} \boldsymbol{D}_{l,l}\boldsymbol{p}_{l,l} + \sigma_l\boldsymbol{i}_{M^2}, & \text{for } i = l, \\ \boldsymbol{D}_{i,l}\boldsymbol{p}_{i,l}, & \text{for } i \neq l, \end{cases} \quad (19)$$

where $\boldsymbol{D}_{i,l} = \boldsymbol{A}_l^* \odot \boldsymbol{A}_i$ and $\boldsymbol{i}_{M^2} = \mathrm{vec}(\boldsymbol{I}_M)$, with $\odot$ denoting the Khatri-Rao product. According to (13), (18), and (19), the derivative of $\bar{\boldsymbol{r}}$ w.r.t. $\boldsymbol{\alpha}^T$ can be deduced as below:

$$\begin{aligned}
&\frac{\partial \bar{\boldsymbol{r}}}{\partial \boldsymbol{\theta}^T} = \boldsymbol{J}\sum_{i=1}^{L}\sum_{l=1}^{L}\left(\boldsymbol{u}_{i,l} \otimes \dot{\boldsymbol{D}}_{i,l}\boldsymbol{P}_{i,l}\right), \\
&\frac{\partial \bar{\boldsymbol{r}}}{\partial \boldsymbol{p}_{1,1}^T} = \boldsymbol{J}\sum_{l=1}^{L}(\boldsymbol{u}_{l,l} \otimes \boldsymbol{D}_{l,l}), \; \frac{\partial \bar{\boldsymbol{r}}}{\partial \sigma_l} = \boldsymbol{J}(\boldsymbol{u}_{l,l} \otimes \boldsymbol{i}_{M^2}), \\
&\frac{\partial \bar{\boldsymbol{r}}}{\partial \mathrm{Re}(\boldsymbol{p}_{i,l}^T)} = \boldsymbol{J}(\boldsymbol{u}_{i,l} \otimes \boldsymbol{D}_{i,l} + \boldsymbol{u}_{l,i} \otimes \boldsymbol{D}_{l,i}), \text{ for } i \neq l, \\
&\frac{\partial \bar{\boldsymbol{r}}}{\partial \mathrm{Im}(\boldsymbol{p}_{i,l}^T)} = \mathrm{j}\boldsymbol{J}(\boldsymbol{u}_{i,l} \otimes \boldsymbol{D}_{i,l} - \boldsymbol{u}_{l,i} \otimes \boldsymbol{D}_{l,i}), \text{ for } i \neq l,
\end{aligned} \quad (20)$$

where $\dot{\boldsymbol{D}}_{i,l} = \dot{\boldsymbol{A}}_l^* \odot \boldsymbol{A}_i + \boldsymbol{A}_l^* \odot \dot{\boldsymbol{A}}_i$ and $\dot{\boldsymbol{A}}_l = [\partial \boldsymbol{a}_l(\theta_1)/\partial\theta_1, \ldots, \partial \boldsymbol{a}_l(\theta_K)/\partial\theta_K]$.

Remark 1: For linear arrays, $\boldsymbol{D}_{i,l}$ can be expressed as

$$\boldsymbol{D}_{i,l} = \boldsymbol{\Psi}_{i,l}\boldsymbol{A}_{\mathrm{d}}^{(i,l)}, \quad (21)$$

where $\boldsymbol{\Psi}_{i,l}$ is an $M^2 \times D_{i,l}$ binary matrix of full column rank [12] with $D_{i,l}$ denoting the number of virtual sensors in the difference co-array constructed by the frequency pair (f_i, f_l), and $\boldsymbol{A}_{\mathrm{d}}^{(i,l)}$ is the difference co-array manifold matrix [28]. Substituting (21) into (20), we know that the row rank of $\partial\bar{\boldsymbol{r}}/\partial\boldsymbol{\alpha}^T$ is $\sum_{i=1}^{L}\sum_{l=1}^{L} D_{i,l}$, while the column rank is $L(L-1)K + 2K + L$. By the information-regularity condition [43], ensuring parameter identifiability requires $\partial\bar{\boldsymbol{r}}/\partial\boldsymbol{\alpha}^T$ to have full column rank, which yields an upper bound on the number of resolvable targets: $K \leq (\sum_{i=1}^{L}\sum_{l=1}^{L} D_{i,l} - L)/(L^2 - L + 2)$.

Using (20), (16), and (17), we can obtain the closed-form CRB expression for a specific L. For example, if $L = 2$, then

$$\begin{aligned}
\boldsymbol{G}|_{L=2} &= \boldsymbol{W}\boldsymbol{J}[\boldsymbol{P}_{1,1}^T\dot{\boldsymbol{D}}_{1,1}^T, \boldsymbol{P}_{2,1}^T\dot{\boldsymbol{D}}_{2,1}^T, \boldsymbol{P}_{1,2}^T\dot{\boldsymbol{D}}_{1,2}^T, \boldsymbol{P}_{2,2}^T\dot{\boldsymbol{D}}_{2,2}^T]^T, \\
\boldsymbol{\Delta}|_{L=2} &= \boldsymbol{W}\boldsymbol{J}\begin{bmatrix} \boldsymbol{D}_{1,1} & \boldsymbol{0} & \boldsymbol{0} & \boldsymbol{i}_{M^2} & \boldsymbol{0} \\ \boldsymbol{0} & \boldsymbol{D}_{2,1} & -\mathrm{j}\boldsymbol{D}_{2,1} & \boldsymbol{0} & \boldsymbol{0} \\ \boldsymbol{0} & \boldsymbol{D}_{1,2} & \mathrm{j}\boldsymbol{D}_{1,2} & \boldsymbol{0} & \boldsymbol{0} \\ \boldsymbol{D}_{2,2} & \boldsymbol{0} & \boldsymbol{0} & \boldsymbol{0} & \boldsymbol{i}_{M^2} \end{bmatrix}.
\end{aligned} \quad (22)$$

Substituting (22) into (17), we can obtain the closed-form CRB expression for the dual-frequency case. The results for different values of L follow the same way.

Compared to the general CRB formula in [35, Eq. B.3.3], our developed CRB expression is more convenient for calculating the CRB for DOA estimation. It also reveals the role of difference co-arrays, thereby suitable for further CRB analyses, including the existence condition [12], [15], [24], the asymptotic behavior w.r.t. signal-to-noise ratio (SNR) [12], [13], and comparisons with mean squared errors [13], [44].

B. Comparison with the Existing CRB for Two Frequencies

In [31], the CRB for a single pair of co-prime frequencies is presented, and the authors consider an ideal signal model with time-invariant phase differences (denoted by ϕ_k', $k = 1, \ldots, K$) and without amplitude variations. The following *a priori* knowledge is introduced:

$$\boldsymbol{s}_2(t) = \boldsymbol{\Phi}\boldsymbol{s}_1(t), \quad (23)$$

where $\boldsymbol{\Phi} = \mathrm{diag}([\mathrm{e}^{\mathrm{j}\phi_1'}, \ldots, \mathrm{e}^{\mathrm{j}\phi_K'}])$ is the additional phase matrix. The overall data vector is given by [31] $\bar{\boldsymbol{x}}'(t) = \bar{\boldsymbol{A}}'\boldsymbol{s}_1(t) + \bar{\boldsymbol{n}}(t)$, where $\bar{\boldsymbol{A}}' = [\boldsymbol{A}_1^T, (\boldsymbol{A}_2\boldsymbol{\Phi})^T]^T$. Thus, the covariance matrix $\bar{\boldsymbol{R}}$ and the unknown parameter vector $\boldsymbol{\alpha}$ respectively change to

$$\begin{aligned}
\bar{\boldsymbol{R}}' &= \bar{\boldsymbol{A}}'\boldsymbol{P}_{1,1}\bar{\boldsymbol{A}}'^H + \bar{\boldsymbol{Q}}, \\
\boldsymbol{\alpha}' &= [\boldsymbol{\theta}^T, \boldsymbol{p}_{1,1}^T, \boldsymbol{\phi}'^T, \sigma_1, \sigma_2]^T,
\end{aligned} \quad (24)$$

with $\boldsymbol{\phi}' = [\phi_1', \ldots, \phi_K']^T$. The CRB can be obtained by substituting (24) into (14) and then taking the inverse.

Comparing $\boldsymbol{\alpha}|_{L=2}$ in (15) with $\boldsymbol{\alpha}'$, we find that the $2K$ unknowns in $\bar{\boldsymbol{p}}$ are reduced to the K ones in $\boldsymbol{\phi}'$, while the others remain the same. In general, less nuisance parameters implies less estimation uncertainty and yields a lower CRB [24, Theorem 1]. Moreover, all the existing methods actually regard $\bar{\boldsymbol{p}}$ as the unknown vector instead of $\boldsymbol{\phi}'$. Whether (23) holds or not, the phase information is ignored, and group sparsity is employed to jointly recover the DOAs [25]–[28]. Consequently, the CRB derived under (23) would be over-optimistic, as also evidenced by a large gap between this CRB

and the empirical root mean square error (RMSE) shown in [31, Fig. 2], where the CRB is $O(10^{-6})$ but the RMSE is $O(10^{-3})$ at 20 dB SNR. In cases where (23) does not hold due to frequent-dependent RCS fluctuations [26], [27], existing algorithms are applicable, whereas the CRB in [31] is not. Instead, our CRB provides a moderate performance benchmark for such cases.

IV. Simulation Results

Consider a 4-sensor ULA with inter-sensor spacing d. The steering vector for the k-th target at f_l is $\boldsymbol{a}_l(\theta_k) = [1, \mathrm{e}^{\mathrm{j}2\pi d\sin(\theta_k)/\lambda_l}, \mathrm{e}^{\mathrm{j}4\pi d\sin(\theta_k)/\lambda_l}, \mathrm{e}^{\mathrm{j}6\pi d\sin(\theta_k)/\lambda_l}]^T$, where $\lambda_l = f_l/c$ with c being the propagation velocity.

The l-th frequency is set as $f_l = \xi_l f_0$, where ξ_l is a positive integer, and f_0 is a common frequency divisor. We choose $d = \lambda_0/2$ and $\lambda_0 = f_0/c$. The powers of the uncontaminated signals $\{y_k^{(l)}(t)\}_{k=1}^K$ are assumed to be identical. The noise powers $\{\sigma_l\}_{l=1}^L$ are also identical.

The group sparsity based DOA estimation algorithm [20] is adopted, which is applicable to both dual-frequency and multi-frequency scenarios. The search grid ranges from $-90°$ to $90°$ with a step size of $0.01°$. Consider $K = 8$ targets located at $\boldsymbol{\theta} = [-58.60°, -40.85°, -26.00°, -7.65°, 8.95°, 26.75°, 44.00°, 59.05°]^T$. The allowable error bound is chosen to give the best estimation results through the trial-and-error approach in every experiment. The empirical RMSE is computed from 100 Monte-Carlo simulations and compared with the averaged CRB for all DOAs, with a varying input SNR from -20 dB to 40 dB and a fixed number of snapshots $N = 2000$.

A. Ideal Case with Two Frequencies

First, our CRB (denoted by B_1) is compared with that in [31] (denoted by B_2) for the ideal case where (23) holds true. Let $\xi_1 = 3$ and $\xi_2 = 4$, which form a coprime pair. The phase difference is set as $\phi_k = 2\pi(k-1)/K$.

In Fig. 1(a), B_1, B_2 and the RMSE have converged to different constants, which implies that increasing SNR will not improve the estimation accuracy when the SNR exceeds certain threshold values. In particular, B_2 is clearly lower than B_1, indicating that our CRB is tighter. This also coincides with the phenomenon that B_2 is much lower than the RMSE curve in [31, Fig. 2]. As explained in Sec. III-B, the phase information is not utilized by existing algorithms, even though (23) holds. During derivation, we regard $\bar{\boldsymbol{p}}$ as the unknown parameter vector instead of $\boldsymbol{\phi}'$, which matches the algorithm and also the general model with frequency-dependent fluctuating RCS, so that our CRB is closer to the RMSE.

B. Practical Case with Multiple Frequencies

Now consider a practical model as described in Sec. II-A with $L = 4$ frequencies and $\xi_1 = 3$, $\xi_2 = 4$, $\xi_3 = 5$, and $\xi_4 = 7$, yielding 6 coprime pairs in total. Assume that the amplitude variations follow the Rayleigh distribution [32], whose mean and variance are respectively set as $\sqrt{\pi/4}$ and $1 - \pi/4$, so that $E[(\rho_k^{(l)})^2(t)] = 1$. The phase difference is set to be time-variant, satisfying $\phi_k(t) = 2\pi(k-1)t/K$. In this case, (23) does not hold, so that B_2 becomes invalid.

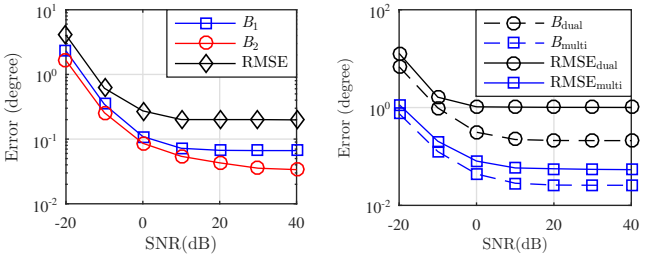

(a) Ideal dual-frequency case. (b) Practical multi-frequency case.

Fig. 1. CRB and RMSE versus SNR in different cases.

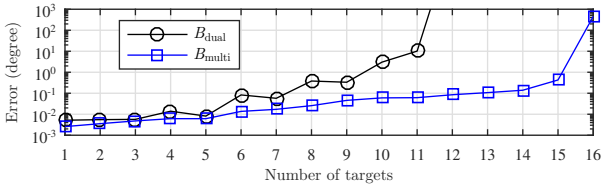

Fig. 2. CRB versus the number of targets.

We compare the CRBs and RMSEs exploiting dual frequencies (f_1, f_2) and all 6 frequency pairs, respectively. As shown in Fig. 1(b), our CRB provides a moderate performance benchmark for the practical case considered here. Clearly, the multi-frequency CRB and RMSE are lower than their dual-frequency counterparts, indicating that using multiple frequencies can significantly improve the estimation accuracy.

C. CRB versus the Number of Targets

Set SNR $= 20$ dB and $N = 2000$, and the dual-frequency and multi-frequency CRBs versus the number of targets (uniformly located in $[-60°, -60°]$) are examined next. The phase differences and amplitude variations are the same as those in the second experiment. Fig. 2 shows that the dual-frequency and multi-frequency CRBs diverge to infinity when K exceeds 11 and 15, respectively. Examining all frequency pairs, we have $\{D_{l,l}\}_{l=1}^L = 7$, $D_{1,2} = D_{2,1} = 19$, $D_{1,3} = D_{3,1} = 23$, $D_{2,3} = D_{3,2} = 25$, $D_{1,4} = D_{4,1} = D_{2,4} = D_{4,2} = D_{3,4} = D_{4,3} = 31$. According to *Remark* 1, the number of resolvable targets cannot exceed 12 and 24 when $L = 2$ and $L = 4$, respectively, which agrees with Fig. 2. In addition, the multi-frequency CRB is always lower than the dual-frequency one, and their distance generally grows larger as K increases.

V. Conclusion

The CRB for DOA estimation exploiting multiple frequency pairs has been derived based on both auto-correlation and cross-correlation information among frequencies. Compared with the existing dual-frequency result, we considered a practical model involving time-variant phase differences and frequency-dependent amplitude variations. The derived CRB provides not only a tighter performance baseline for existing algorithms exploiting two frequencies, but also a benchmark for the first time for the multi-frequency scenario. As demonstrated by simulations, using more frequency pairs has yielded a lower CRB while simultaneously resolving more targets.

REFERENCES

[1] P. Pal and P. Vaidyanathan, "Nested arrays: A novel approach to array processing with enhanced degrees of freedom," *IEEE Trans. Signal Process.*, vol. 58, no. 8, pp. 4167–4181, 2010.

[2] P. P. Vaidyanathan and P. Pal, "Sparse sensing with co-prime samplers and arrays," *IEEE Trans. Signal Process.*, vol. 59, no. 2, pp. 573–586, 2011.

[3] S. Qin, Y. D. Zhang, and M. G. Amin, "Generalized coprime array configurations for direction-of-arrival estimation," *IEEE Trans. Signal Process.*, vol. 63, no. 6, pp. 1377–1390, 2015.

[4] P. Pal and P. P. Vaidyanathan, "Coprime sampling and the MUSIC algorithm," in *Proc. Digital Signal Process. Workshop and IEEE Signal Process. Educ. Workshop (DSP/SPE)*. IEEE, 2011, pp. 289–294.

[5] M. Guo, Y. D. Zhang, and T. Chen, "DOA estimation using compressed sparse array," *IEEE Trans. Signal Process.*, vol. 66, no. 15, pp. 4133–4146, 2018.

[6] C.-L. Liu and P. Vaidyanathan, "Super nested arrays: Linear sparse arrays with reduced mutual coupling—Part I: Fundamentals," *IEEE Trans. Signal Process.*, vol. 64, no. 15, pp. 3997–4012, 2016.

[7] A. Raza, W. Liu, and Q. Shen, "Thinned coprime array for second-order difference co-array generation with reduced mutual coupling," *IEEE Trans. Signal Process.*, vol. 67, no. 8, pp. 2052–2065, 2019.

[8] Q. Shen, W. Liu, W. Cui, S. Wu, and P. Pal, "Simplified and enhanced multiple level nested arrays exploiting high-order difference co-arrays," *IEEE Trans. Signal Process.*, vol. 67, no. 13, pp. 3502–3515, 2019.

[9] Q. Shen, W. Liu, W. Cui, and S. Wu, "Extension of co-prime arrays based on the fourth-order difference co-array concept," *IEEE Signal Process. Lett.*, vol. 23, no. 5, pp. 615–619, 2016.

[10] Y. D. Zhang, M. G. Amin, and B. Himed, "Sparsity-based DOA estimation using co-prime arrays," in *Proc. IEEE Int. Conf. Acoust., Speech, Signal Process. (ICASSP)*. IEEE, 2013, pp. 3967–3971.

[11] H. Qiao and P. Pal, "On maximum-likelihood methods for localizing more sources than sensors," *IEEE Signal Process. Lett.*, vol. 24, no. 5, pp. 703–706, 2017.

[12] C.-L. Liu and P. Vaidyanathan, "Cramér-Rao bounds for coprime and other sparse arrays, which find more sources than sensors," *Digital Signal Process.*, vol. 61, pp. 43–61, 2017.

[13] M. Wang and A. Nehorai, "Coarrays, MUSIC, and the Cramér-Rao bound," *IEEE Trans. Signal Process.*, vol. 65, no. 4, pp. 933–946, 2017.

[14] M. Wang, Z. Zhang, and A. Nehorai, "Performance analysis of coarray-based MUSIC in the presence of sensor location errors," *IEEE Trans. Signal Process.*, vol. 66, no. 12, pp. 3074–3085, 2018.

[15] A. Koochakzadeh and P. Pal, "Cramér-Rao bounds for underdetermined source localization," *IEEE Signal Process. Lett.*, vol. 23, no. 7, pp. 919–923, 2016.

[16] A. Koochakzadeh and P. Pal, "Performance of uniform and sparse non-uniform samplers in presence of modeling errors: A Cramér-Rao bound based study," *IEEE Trans. Signal Process.*, vol. 65, no. 6, pp. 1607–1621, 2016.

[17] K. Han and A. Nehorai, "Wideband Gaussian source processing using a linear nested array." *IEEE Signal Process. Lett.*, vol. 20, no. 11, pp. 1110–1113, 2013.

[18] Q. Shen, W. Liu, W. Cui, S. Wu, Y. D. Zhang, and M. G. Amin, "Low-complexity direction-of-arrival estimation based on wideband co-prime arrays," *IEEE/ACM Trans. Audio, Speech, Language Process.*, vol. 23, no. 9, pp. 1445–1453, 2015.

[19] Q. Shen, W. Cui, W. Liu, S. Wu, Y. D. Zhang, and M. G. Amin, "Underdetermined wideband DOA estimation of off-grid sources employing the difference co-array concept," *Signal Process.*, vol. 130, pp. 299–304, 2017.

[20] Q. Shen, W. Liu, W. Cui, and S. Wu, "Underdetermined DOA estimation under the compressive sensing framework: A review," *IEEE Access*, vol. 4, pp. 8865–8878, 2016.

[21] E. BouDaher, Y. Jia, F. Ahmad, and M. G. Amin, "Multi-frequency co-prime arrays for high-resolution direction-of-arrival estimation," *IEEE Trans. Signal Process.*, vol. 63, no. 14, pp. 3797–3808, 2015.

[22] W. Cui, Q. Shen, W. Liu, and S. Wu, "Low complexity DOA estimation for wideband off-grid sources based on re-focused compressive sensing with dynamic dictionary," *IEEE J. Sel. Topics Signal Process.*, vol. 13, no. 5, pp. 918–930, 2019.

[23] Y. Liang, Q. Shen, W. Cui, and W. Liu, "Cramér-Rao bound for wideband DOA estimation with uncorrelated sources," in *Proc. IEEE Global Conf. Signal Inf. Process. (GlobalSIP)*. IEEE, 2019, pp. 1–5.

[24] Y. Liang, W. Liu, Q. Shen, W. Cui, and S. Wu, "A review of closed-form Cramér-Rao bounds for DOA estimation in the presence of Gaussian noise under a unified framework," *IEEE Access*, vol. 8, pp. 175 101–175 124, 2020.

[25] Y. D. Zhang, M. G. Amin, F. Ahmad, and B. Himed, "DOA estimation using a sparse uniform linear array with two CW signals of co-prime frequencies," in *Proc. 5th IEEE Int. Workshop Comput. Adv. Multi-Sensor Adaptive Process. (CAMSAP)*, 2013, pp. 404–407.

[26] Q. Shen, W. Liu, W. Cui, S. Wu, Y. D. Zhang, and M. G. Amin, "Wideband DOA estimation for uniform linear arrays based on the co-array concept," in *Proc. 23rd European Signal Process. Conf. (EUSIPCO)*. IEEE, 2015, pp. 2835–2839.

[27] H. Wu, Q. Shen, W. Liu, and W. Cui, "Underdetermined low-complexity wideband DOA estimation with uniform linear arrays," in *Proc. Sensor Array Multichannel Signal Process. Workshop (SAM)*, 2020, pp. 1–5.

[28] S. Qin, Y. D. Zhang, M. G. Amin, and B. Himed, "DOA estimation exploiting a uniform linear array with multiple co-prime frequencies," *Signal Process.*, vol. 130, pp. 37–46, 2017.

[29] A. Ahmed, D. Silage, and Y. D. Zhang, "High-resolution target sensing using multi-frequency sparse array," in *Proc. IEEE Sensor Array Multichannel Signal Process. Workshop (SAM)*, 2020, pp. 1–5.

[30] S. Zhang, A. Ahmed, Y. D. Zhang, and S. Sun, "DOA estimation exploiting interpolated multi-frequency sparse array," in *Proc. IEEE Sensor Array Multichannel Signal Process. Workshop (SAM)*, 2020, pp. 1–5.

[31] M. Guo, Y. D. Zhang, and T. Chen, "Performance analysis for uniform linear arrays exploiting two coprime frequencies," *IEEE Signal Process. Lett.*, vol. 25, no. 6, pp. 838–842, 2018.

[32] P. Swerling, "Probability of detection for fluctuating targets," *IRE Trans. Inf. Theory*, vol. 6, no. 2, pp. 269–308, 1960.

[33] C. Uluisik, G. Cakir, M. Cakir, and L. Sevgi, "Radar cross section (RCS) modeling and simulation, Part 1: A tutorial review of definitions, strategies, and canonical examples," *IEEE Antennas Propag. Mag.*, vol. 50, no. 1, pp. 115–126, 2008.

[34] M. I. Skolnik, *Radar Handbook*. New York, NY, USA: McGraw-Hill, 2008.

[35] P. Stoica and R. L. Moses, *Spectral Analysis of Signals*. Upper Saddle River, NJ, USA: Pearson Prentice Hall, 2005.

[36] B. Ottersten, M. Viberg, P. Stoica, and A. Nehorai, "Exact and large sample maximum likelihood techniques for parameter estimation and detection in array processing," in *Radar Array Process.* Springer, 1993, pp. 99–151.

[37] D. R. Brillinger, *Time Series: Data Analysis and Theory*. Philadelphia, PA, USA: Society for Industrial and Applied Mathematics, 2001.

[38] E. Ollila, D. E. Tyler, V. Koivunen, and H. V. Poor, "Complex elliptically symmetric distributions: Survey, new results and applications," *IEEE Trans. Signal Process.*, vol. 60, no. 11, pp. 5597–5625, 2012.

[39] H. Abeida and J.-P. Delmas, "Slepian–Bangs formula and Cramér–Rao Bound for circular and non-circular complex elliptical symmetric distributions," *IEEE Signal Process. Lett.*, vol. 26, no. 10, pp. 1561–1565, 2019.

[40] P. Stoica, E. G. Larsson, and A. B. Gershman, "The stochastic CRB for array processing: A textbook derivation," *IEEE Signal Process. Lett.*, vol. 8, no. 5, pp. 148–150, 2001.

[41] R. H. Koning, H. Neudecker, and T. Wansbeek, "Block Kronecker products and the vecb operator," *Linear Algebra Appl.*, vol. 149, pp. 165–184, 1991.

[42] H. Lütkepohl, *Handbook of Matrices*. Chichester, West Sussex, UK: John Wiley & Sons, 1996.

[43] B. Hochwald and A. Nehorai, "On identifiability and information-regularity in parametrized normal distributions," *Circuits, Syst. Signal Process.*, vol. 16, no. 1, pp. 83–89, 1997.

[44] P. Stoica and A. Nehorai, "Performance study of conditional and unconditional direction-of-arrival estimation," *IEEE Trans. Acoust., Speech, Signal Process.*, vol. 38, no. 10, pp. 1783–1795, 1990.